

1 **Temporal variability of tropospheric ozone and ozone**  
2 **profiles in Korean Peninsula during the East Asian**  
3 **summer monsoon: Insights from multiple**  
4 **measurements and reanalysis datasets**

5  
6 Juseon Bak<sup>1,\*</sup>, [juseonbak@pusan.ac.kr](mailto:juseonbak@pusan.ac.kr)

7 Eun-Ji Song<sup>1,a</sup>, [ejsong0510@gmail.com](mailto:ejsong0510@gmail.com)

8 Hyo-Jung Lee<sup>1</sup>, [hyojung@pusan.ac.kr](mailto:hyojung@pusan.ac.kr)

9 Xiong Liu<sup>2</sup>, [xliu@cfa.harvard.edu](mailto:xliu@cfa.harvard.edu)

10 Ja-Ho Koo<sup>3</sup>, [zach45@yonsei.ac.kr](mailto:zach45@yonsei.ac.kr)

11 Joowan Kim<sup>4</sup>, [joowan@kongju.ac.kr](mailto:joowan@kongju.ac.kr)

12 Wonbae Jeon<sup>1,5</sup>, [wajeon@pusan.ac.kr](mailto:wajeon@pusan.ac.kr)

13 Jae-Hwan Kim<sup>5</sup>, [jaekim@pusan.ac.kr](mailto:jaekim@pusan.ac.kr)

14 Cheol-Hee Kim<sup>1,5,\*</sup>, [chkim2@pusan.ac.kr](mailto:chkim2@pusan.ac.kr)

15  
16 <sup>1</sup>*Institute of Environmental Studies, Pusan National University, Busan, South Korea*

17 <sup>2</sup>*Smithsonian Astrophysical Observatory (SAO), Center for Astrophysics | Harvard & Smithsonian,*  
18 *Cambridge, MA 02138, USA*

19 <sup>3</sup>*Department of Atmospheric Sciences, Yonsei University, Seoul, Republic of Korea*

20 <sup>4</sup>*Department of Atmospheric Sciences, Kongju National University, Kongju, South Korea*

21 <sup>5</sup>*Department of Atmospheric Sciences, Pusan National University, Busan, South Korea*

22 <sup>a</sup>*Currently at Supercomputer Center, Pukyong National University, Busan, South Korea*

23  
24 *Corresponding Author\**  
25  
26  
27  
28  
29

## Abstract

We investigate the temporal variations of the ground-level ozone and balloon-based ozone profiles at Pohang (36.02°N, 129.23°E) in Korean Peninsula. Satellite measurements and chemical reanalysis products are also intercompared to address their capability of providing a consistent information on the temporal and vertical variability of atmospheric ozone. Sub-seasonal variations of the summertime lower tropospheric ozone exhibit a bimodal pattern related to atmospheric weather patterns modulated by the East Asian monsoon circulation. The peak ozone abundances occur during the pre-summer monsoon with enhanced ozone formation due to favorable meteorological conditions (dry and sunny). Ozone concentrations reach its minimum during the summer monsoon and then reemerges in autumn before the winter monsoon arrives. Profile measurements indicates that ground-level ozone is vertically mixed up 400 hPa in summer while the impact of the summer monsoon on ozone dilution is found up to 600 hPa. Compared to satellite measurements, reanalysis products largely overestimate ozone abundances in both troposphere and stratosphere and give inconsistent features of temporal variations. Nadir-viewing measurements from the Ozone Monitoring Instrument (OMI) slightly underestimate the boundary layer ozone, but well represent the bimodal peaks of ozone in the lower troposphere and the interannual changes of the lower tropospheric ozone in August, with higher ozone concentrations during the strong El Niño events and the low ozone concentrations in during the 2020 La Niña event.

## 1. Introduction

Ozone in the lower troposphere should be reduced due to its adverse effect as a key air pollutant and greenhouse gas, whereas stratospheric ozone should be protected for life on the Earth due to its essential role in shielding harmful ultraviolet (UV) rays from the sun. The human activities damage the protective layer of the stratosphere with emissions of ozone-depleting substances (halogen source gases) as well as cause emissions of tropospheric ozone precursors (nitrogen oxides, volatile organic compounds), which chemically react in the presence of sunlight producing tropospheric ozone. The photochemical formation and fate of ozone in the troposphere is complicatedly interacted with meteorology and climate variability (Jacob and Winner, 2009; Lu et al., 2019; Zhang and Wang, 2016), making it difficult to evaluate impacts of the emission control measures on surface ozone levels (Dufour et al., 2021). As well, the tropospheric ozone is strongly influenced by either downward transport of stratospheric air masses or the horizontal transport of polluted air-masses (Langford et al., 2015; Walker et al., 2010).

60 A monsoon is a major atmospheric circulation system affecting air mass transport, convection, and  
61 precipitation in the middle and high latitudes. Lower tropospheric ozone and its precursors can be  
62 significantly modulated by monsoonal changes on the physical and chemical processes to production, and  
63 deposition and redistribution. The regional seasonality of ozone as well as the latitudinal differences in  
64 ozone seasonality were attributed to the Asian monsoon-driven atmospheric circulation (Worden et al.,  
65 2009). In particular, impacts of the East Asian summer monsoon (EASM) on spatiotemporal variations of  
66 surface-layer ozone concentrations over China have been comprehensively addressed (Gao et al., 2021; He  
67 et al., 2008; Li et al., 2018; Shen et al., 2022; Yang et al., 2014; Yin et al., 2019; Zhao et al., 2010). For  
68 example, Yin et al., (2019) characterized the geographical distribution of ozone in China, with a bimodal  
69 structure of ozone with a summer trough in the southern China whereas a unimodal cycle in the northern  
70 China. Shen et al. (2022) specified the source-receptor relationships of ozone pollution over the central and  
71 eastern China, mainly modulated by the monsoon circulation.

72 In view of the rainfall characteristics during EASM and its impact on tropospheric ozone over East Asia,  
73 Korean Peninsula is one of the best regions worldwide. Korean Peninsula is located in the easternmost part  
74 of the Asian continent adjacent to the West Pacific where more than a half of the total rainfall amount  
75 is typically concentrated during a short rainy season called Jangma in summer, largely controlled by  
76 the EASM (Choi et al., 2020; Ha et al., 2012). Therefore, understanding the EASM-induced changes in  
77 chemical composition over the Korean peninsula is of importance, which has rarely been done in literature,  
78 especially for ozone.

79 The main objective of this paper is to characterize the temporal variability of tropospheric ozone and  
80 ozone profiles, by linking with the meteorological variability largely controlled by the EASM. Ground-  
81 based and balloon-based observations are collected from the Pohang station (36.02°N, 129.23°E) as a  
82 reference dataset. The ground measurements are used to interpret the sub-seasonal variability of surface  
83 ozone, while the vertical seasonality of ozone is investigated from ozonesondes. This paper is a preliminary  
84 activity of the Asian Summer Monsoon Chemical and Climate Impact Project (ACCLIP) campaign  
85 (<https://www2.acom.ucar.edu/acclip>) to investigate the impact of the Asian Summer Monsoon on regional  
86 and global chemistry. The ACCLIP campaign will operate two aircrafts during the period July to August  
87 in 2022 to measure atmospheric compounds through entire troposphere to lower troposphere over East Asia  
88 and the West Pacific. The second objective of this paper is to evaluate whether the chemical reanalysis data  
89 and remote-sensing data could represent a consistent picture of the summer monsoon impact on ozone  
90 profile distribution. This evaluation will give an insight on the data selection used to fill in

91 the spatiotemporal gaps of the ACCLIP measurements.

92

## 93 **2. Data descriptions**

### 94 **2.1 Ground measurements**

95 Surface in-situ measurements of O<sub>3</sub> and NO<sub>2</sub> are collected from air quality monitoring networks of the  
96 National Institute of Environmental Research (NIER) (AirKorea, <http://www.airkorea.or.kr>). This network  
97 measures hourly air pollutants (O<sub>3</sub>, NO<sub>2</sub>, CO, SO<sub>2</sub>) mixing ratios through the chemiluminescence  
98 technology (Kley and Mcfarland, 1980). The KMA operates automatic synoptic observation system (ASOS)  
99 at 102 weather stations. The ASOS measurements are provided in five types of time scales (minutely, hourly,  
100 daily, monthly, yearly) via the KMA Weather Data Service (<https://data.kma.go.kr/>). We used daily  
101 averages of air temperature, relative humidity, solar irradiance, total precipitation, wind speed, and wind  
102 direction.

### 103 **2.2 Ozonesonde measurements**

104 Ozonesondes are balloon-borne instruments capable of measuring the vertical distribution  
105 of atmospheric ozone from the surface to balloon burst, usually near 35 km. The electrochemical  
106 concentration cell (ECC)-typed sensor is the most widely employed. ECC ozonesondes have an uncertainty  
107 of 5 %–10 % and a precision of 3 %–5 % (Smit et al., 2007). In South Korea, only at the Pohang station  
108 ECC sondes have been regularly launched every Wednesday in the afternoon (13:30-15:30 LT) since 1995.  
109 Ozonesonde measurements are reported in units of partial pressure (mPa) with vertical resolution of about  
110 100 m by the Korea Meteorological Administration (KMA). Bak et al., (2019) demonstrated that Pohang  
111 ozonesondes measurements are a stable set of reference profiles for validating satellite products, with the  
112 comparable quality of ECC ozonesonde measurements in Japan and Hong Kong. To improve the data  
113 quality, we screened out sounding measurements at the balloon burst altitudes higher than 200 hPa,  
114 and observations of either tropospheric ozone column values above 80 DU or stratospheric ozone  
115 column values below 100 DU.

### 116 **2.3 Satellite measurements**

117 Both OMI and MLS were launched on board of NASA's EOS-Aura spacecraft in July 2004 and  
118 still functioning in measuring the Earth's atmospheric composition. The Aura satellite crosses the equator

119 at ~ 1:30 in the afternoon. OMI is a nadir-viewing imaging spectrometer capable of daily, global mapping  
120 at relatively high spatial resolution of  $13 \text{ km} \times 24\text{-}48 \text{ km}$  (across  $\times$  along track). MLS measures microwave  
121 thermal emission from the limb of Earth's atmosphere. Compared to OMI, MLS makes measurements at a  
122 good vertical resolution ( $\sim 3 \text{ km}$ ) in the upper atmosphere, but at relatively coarse horizontal resolutions  
123 ( $\sim 165 \text{ km}$  along the orbit track). The version 4.2 of the MLS standard ozone product is used in this study,  
124 only for the recommended vertical range from 261 to 0.025 hPa (Schwartz et al., 2015). We used OMI  
125 ozone profiles retrieved using the PROFOZ version 2 algorithm which is in preparation for reprocessing  
126 OMI measurements to release a new version of the OMPROFOZ research product (Liu et al., 2010). This  
127 retrieval algorithm consists of wavelength/radiometric calibrations and forward modeling simulations, with  
128 an optimal estimation inversion where a priori knowledge is optimally combined with measurement  
129 information to obtain a better estimate of the state (Rodgers, 2000). The measurement sensitivity inherently  
130 decreases toward the surface, with the increasing dependence of retrievals on the a priori information (Bak  
131 et al., 2013). OMI sensitivity is very low to surface ozone, with its maximum in the free troposphere ( $\sim 500$   
132 hPa) (Shen et al., 2019).

#### 133 **2.4 Reanalysis data**

134 The Modern-Era Retrospective Analysis for Research and Applications, version 2 (MERRA-2), is  
135 NASA's latest reanalysis, spanning the satellite observing era from 1980 to the present (Gelaro et al.,  
136 2017). In addition to a standard meteorological analysis, a global  $\text{O}_3$  field is driven by atmospheric  
137 dynamics and constrained by satellite  $\text{O}_3$  measurements using the GEOS-5 atmospheric model and the data  
138 assimilation system. Beginning in October 2004, MERRA-2 assimilates total column ozone from OMI and  
139 stratospheric ozone profiles above 215 hPa from MLS. Note that OMI total column ozone is assimilated to  
140 account for the lower sensitivity of MLS measurements in the lower stratosphere, specifically in clouded  
141 scenes.

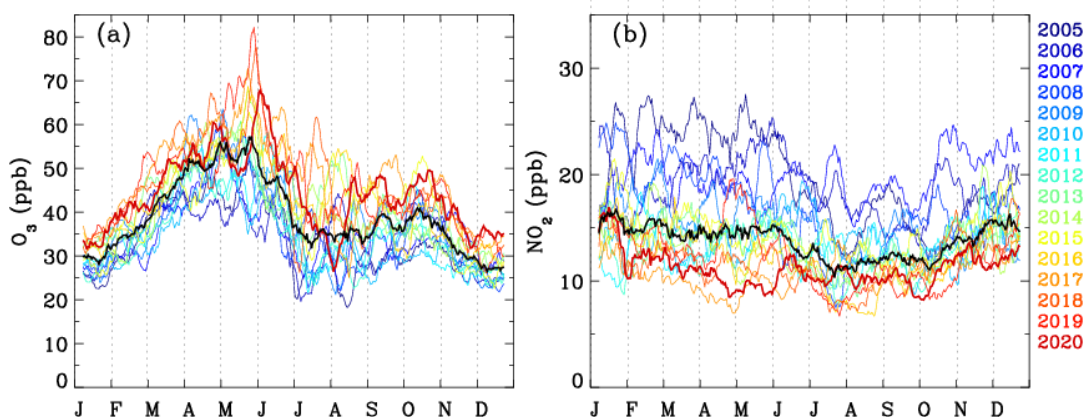
142 The CAMS reanalysis is the latest global reanalysis data set of atmospheric composition produced by the  
143 Copernicus Atmosphere Monitoring Service (CAMS), covering the period from 2003 to present (Inness et  
144 al., 2019). Compared to MERRA-2, multiple satellite measurements were assimilated for the CAMS  
145 reanalysis with ECMWF's Integrated Forecasting System. These included total ozone columns from  
146 SCIAMARCY, OMI, and GOME/2 as well as ozone profiles from MIPAS and MLS after 2005.

147 Both reanalysis data have similar temporal and spatial resolutions. Merra-2 system produces 3-hourly  
148 analyses at 72 sigma-pressure hybrid layers between the surface and 0.01 hPa, with a  
149 horizontal resolution of  $0.625^\circ \times 0.5^\circ$ . The CAMS reanalysis data provide estimates every 3 hours with a

150 horizontal resolution of  $0.75^\circ \times 0.75^\circ$ . The vertical resolution of model consists of 60 hybrid sigma–pressure  
151 (model) levels from surface to 0.1 hPa. In this study, we used CAMS global reanalysis (EAC4) monthly  
152 averaged fields at 25 pressure levels (1000 hPa to 1 hPa) as well as MERRA-2 monthly mean data at 42  
153 pressure levels (1000 hPa to 1 hPa). Both datasets provide ozone profiles in the unit of mixing ratio.

### 154 3. Results and discussion

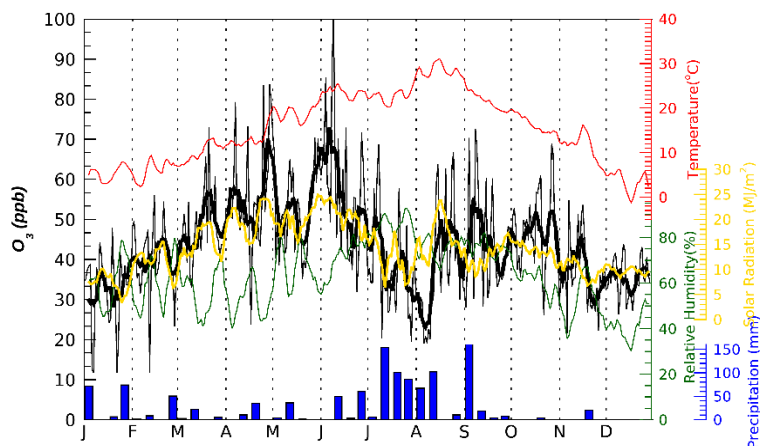
#### 155 3.1. Temporal variability of ground-level ozone



156  
157 **Figure 1.** (a) Two-week moving averages of daytime ground-level ozone concentrations monitored at 6  
158 sites in Pohang, with (b) corresponding  $\text{NO}_2$  concentrations. Different colorings represent each year from  
159 2005 to 2020, while the black line represents the mean ozone concentrations from all years.

160  
161 Figure 1 shows both interannual and seasonal changes of daily ground-level concentrations of  $\text{O}_3$   
162 averaged at six AirKorea sites located within Pohang for 16 years (2005-2020) in comparison with its  
163 primary precursor  $\text{NO}_2$ . Pohang is a major industrial city on South Korea's east coast, with the largest  
164 population of North Gyeongsang Province. In this analysis, hourly measurements in afternoon (1-3 pm  
165 local time) are first averaged for a given calendar day and then smoothed by two-week moving average.  
166 The afternoon  $\text{NO}_2$  do not change much seasonally. However, the seasonal cycle of ozone is bimodal with  
167 peaks in early-summer and fall. Ozone concentration rapidly increases from  $\sim 30$  ppb in January to primary  
168 peak values of  $\sim 55$  ppb on average during the period of late May to early June. The second peak of ozone  
169 occurs in fall, which is much lower than the major peak.

170 In wintertime, the annual minimum of ozone concentrations gradually increases by  $\sim 10$  ppb during  
171 last 15 years whereas the annual maximum of summertime ozone rapidly increases from  $\sim 40$  ppb to 80  
172 ppb, in spite of the reduction of  $\text{NO}_2$  amount by  $\sim 15$  ppb or larger.



173

174 **Figure 2.** (Black) Daily ground-level ozone concentrations where weekly moving averages are applied  
 175 (thick line) or not (thin line) at Pohang in 2020. The corresponding meteorological factors are overpotted;  
 176 surface air temperature (red, °C), solar radiation (yellow, MJ/m<sup>2</sup>), and relative humidity (dark green, %).  
 177 The bar graph shows the total precipitation (mm) for each week.

178 **Table 1.** Same as Figure2, but for correlation coefficients between ozone and meteorological variables, for  
 179 pre-summer, summer, and post-summer periods, respectively.

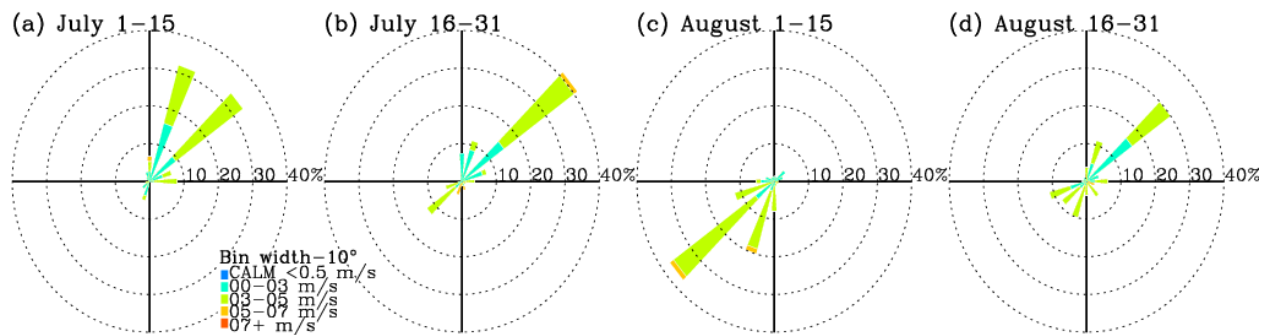
	pre-summer (Jan-May)	Summer (Jun-Aug)	Post-summer (Sep-Dec)
Solar radiation	0.91	0.74	0.51
Air temperature	0.79	-0.15	0.69
Relative humidity	-0.27	-0.64	0.59

180

181 In order to avoid smoothing out important features of intra-summer variations in ozone and their  
 182 association with synoptic weather patterns, daily ozone and meteorological variables are zoomed in 2020  
 183 as one-week moving average (Figure 2). The local maximum of ozone concentrations is generally tied to  
 184 the local warm, dry air and intense solar radiation before the rainy season starts.

185 The correlation between ozone concentrations and meteorological variables is quantitatively compared  
 186 in Table 1, for summer and post/pre-summer periods, respectively. Solar insolation amounts are directly  
 187 linked to ozone concentrations over all seasons ( $r=0.51-0.91$ ). The significant relationship between ozone  
 188 and air temperature is also identified before and after summer seasons. However, in summer, ozone  
 189 variations are rarely linked with temperature variations, due to the intense precipitation suppressing ozone  
 190 formation. Consequently, the local minimum of ozone levels is tied to the local maximum of the relative  
 191 humidity during the rainy season ( $r=-0.64$ ). This is indicating that both depth and width of the summer  
 192 trough could be highly variable, likely influenced by the strength and duration of the summer monsoon

193 (Yang et al., 2014; Zhou et al., 2022). Note that the relative humidity is significantly influenced by air  
 194 temperature, rather than amount of water vapor in the pre and post summer periods. Therefore, in the post  
 195 summer the correlation of ozone with relative humidity ( $r=0.59$ ) is likely to arise from the correlation of  
 196 ozone with air temperature ( $r=0.51$ ). The rapid drop of  $\sim 10$  ppb in ozone from the end of July to early  
 197 August is hardly explained with meteorological factors mentioned above; the weather becomes warmer  
 198 with other meteorological variables (precipitation and solar radiation) being relatively invariant. However,  
 199 the prevailing wind is characterized as southwesterlies in early August, exceptionally. Note that the  
 200 northwesterly winds were dominant in July and in late August (see. Figure 3). This summer minimum could  
 201 deepen with the inflow of the poor ozone airmass originated from the southern sea off the Korean peninsula  
 202 into inland.



203  
 204 **Figure 3.** Wind roses for individual months from June through September in 2020 at Pohang. Note that  
 205 hourly observations in daytime are used to be consistent with data processing done in Figures 1 and 2.

206

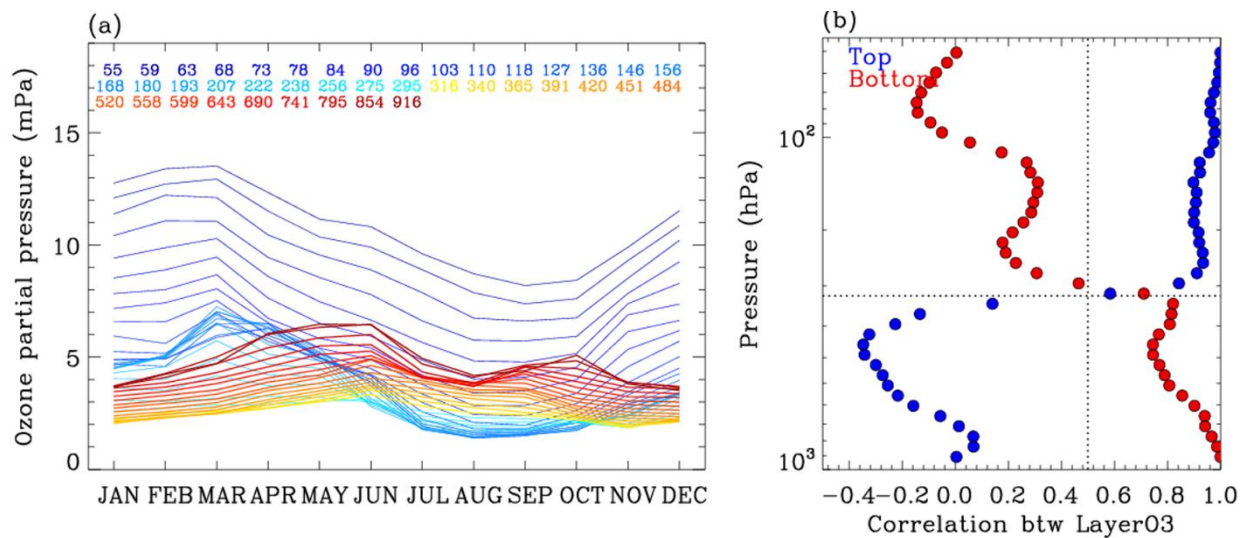
### 207 3.2. Temporal variability of ozone profiles

208 To understand the seasonality of ozone profiles, ozonesonde measurements collected at Pohang station  
 209 are climatologically averaged for each month and each pressure bin ( $\sim 0.5$  km intervals). Ozonesondes  
 210 soundings mainly measure ozone in the lower atmosphere below 10hPa while space-based limb soundings  
 211 mainly measure ozone in the upper atmosphere above 215hPa. However, both sounding measurements  
 212 provide the limited spatiotemporal information. OMI nadir measurements and reanalysis data provide the  
 213 daily global maps of ozone profiles. but the reliability of those data products should be assured before using  
 214 them to interpret ozone variability and its linkage to the monsoon circulation. As shown in Figure 4a, two  
 215 kinds of seasonal patterns are identified with a bimodal structure of layer ozone partial pressures in the  
 216 lower troposphere (LT) whereas a unimodal cycle in the upper troposphere and lower stratosphere (UTLS).



217 The LT ozone concentrations are peaked at June and October with a global minimum in winter as well as  
 218 a local summer minimum in late July and early August, which is consistent with surface measurements.  
 219 The concentrations of UTLS ozone are relatively higher in March due to the stratospheric intrusion, while  
 220 the minimum concentrations appear broadly over the summer and early fall due to the rise of the tropopause,  
 221 which is a common feature of ozone in the extratropical UTLS (Gettelman et al., 2011; Rao et al., 2003).  
 222 In order to quantify the similarity of seasonal variations, the correlation coefficient is calculated for  
 223 temporal ozone changes between each layer and the top/bottom layer. As shown in Fig. 4. b. the seasonality  
 224 of ozone at 50 hPa is significantly correlated down to ~ 300 hPa, with the correlation coefficient of larger  
 225 than 0.8. In addition, ozone in the boundary layer is significantly correlated with the lower tropospheric  
 226 ozone up to 700 hPa ( $r > 0.9$ ) as well as the upper tropospheric ozone up to ~ 300 hPa ( $r = 0.7-0.8$ ). It illustrates  
 227 that the 300 hPa could be regarded as a chemical barrier working as a boundary between troposphere and  
 228 stratosphere at Pohang.

229



230

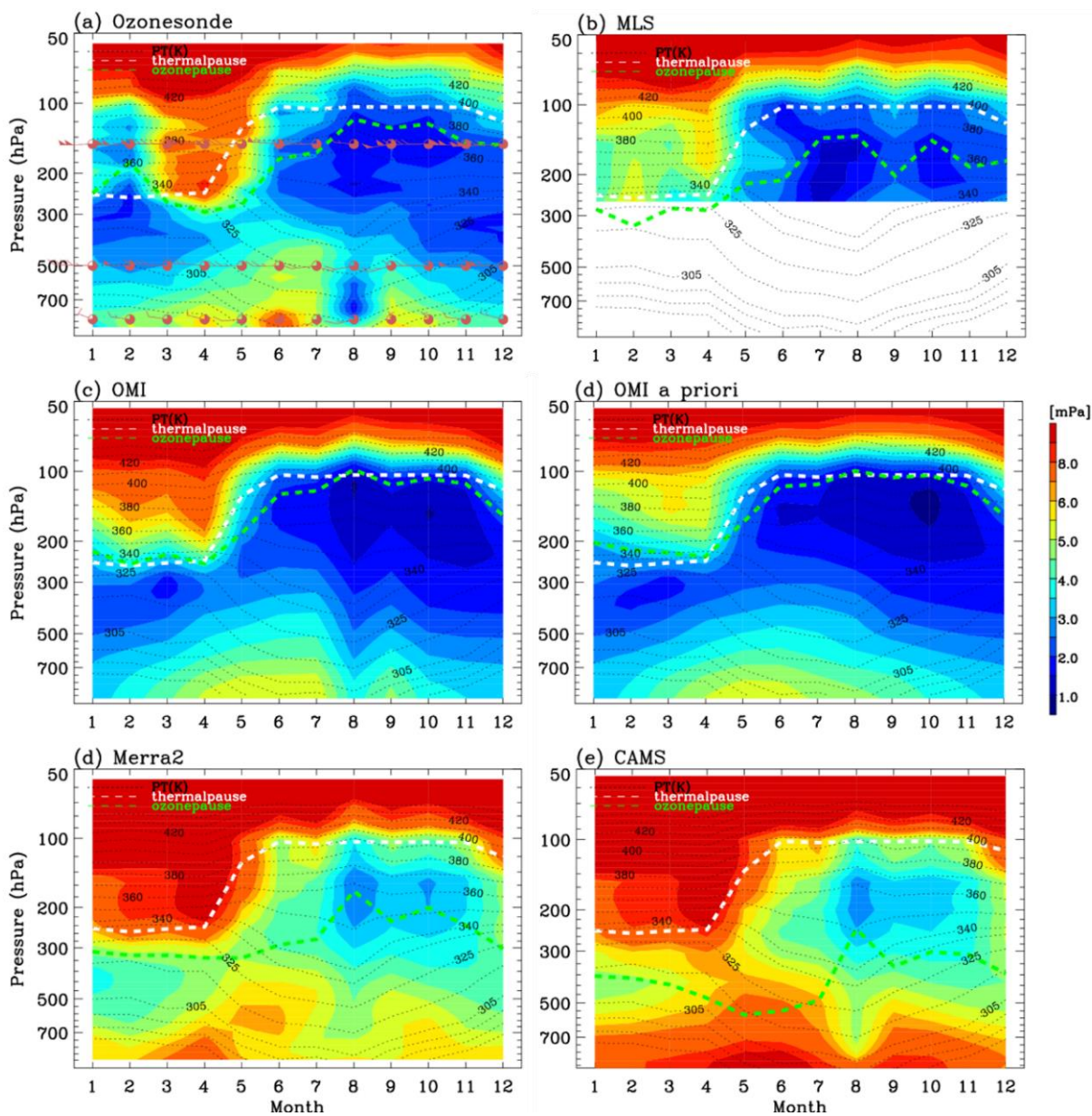
231 **Figure 4.** (a) Monthly variations of layer ozone partial pressures from ozonesonde soundings obtained from  
 232 Pohang during the period of 2005 to 2020. The legend values indicate the midpoint pressure of the layer  
 233 (hPa). (b) Correlation coefficients of monthly ozone variations between each layer and bottom layer (916  
 234 hPa in red)/top layer (55 hPa in green).

235 In Figure 5, monthly averaged ozonesonde profiles are presented for 2020 and compared as a reference  
 236 to assess satellite measurements and reanalysis products. This contour map of ozonesondes clearly  
 237 illustrates the intrusion depth of the stratospheric air masses down to ~ 300 hPa during spring months (Fig  
 238 5a). The mixing depth of ozone that forms near the ground level is also identified, which is bounded up to  
 239 ~400 hPa in the summer and ~600 hPa in other seasons. The minimum ozone concentration is typically

240 found just below the thermal tropopause. The August minimum of the lower tropospheric ozone is vertically  
241 extended above ~600 hPa. This air mass is much cleaner compared to the winter ozone concentration over  
242 the lower troposphere. The dominant factor suppressing the ozone formation is a long-lasting summer  
243 precipitation from early July to mid-Aug in 2020 (Fig.2). Southerly wind that blows on the observation site  
244 is relatively strong compared to June and July. Therefore, we could interpret that the inland polluted air  
245 masses are likely to be diluted with the inflows of the maritime clean air masses as mentioned above. In the  
246 lower troposphere, the minor peak of ozone concentrations is also identified in spring, which is not visible  
247 in time-series plots of surface measurements (Fig. 2). The springtime peak is mainly originated by the fair  
248 weather accelerating the formation of ground-level ozone with the wintertime accumulation of ozone and  
249 its processors; it could be partly attributed by the dynamical processes transporting the ozone-rich airs from  
250 the UTLS and upwind areas. In Figures 5.b-f, OMI, MERRA-2, and CAMS ozone profiles are qualitatively  
251 evaluated with respect to the capability of reproducing the seasonality of ozone profiles at this location.  
252 The ozone minimum of summer monsoon season is detected from all ozone products, but much broader  
253 than that in ozonesondes due to both the limited time resolution of ozonesonde measurements and the  
254 limited spatial resolution of OMI and reanalysis products. OMI also show a very good agreement with  
255 ozonesonde in terms of reproducing the boundary layer ozone extending up to free troposphere and low  
256 ozone concentration below the tropopause. In addition, the vertical gradient of ozone enhancement above  
257 the tropopause is consistently reproduced from OMI, ozonesondes, and MLS. The spring ozone peak near  
258 surface is not detectable from OMI measurements due to the limited sensitivity to relatively shallow  
259 boundary layers compared to summer (Shen et al., 2019). In Figure 5.d, OMI a priori profile is also  
260 presented to highlight that the summer minimum is derived from the independent information of OMI  
261 measurements, rather than a priori information. It also illustrates that the summer minimum is a regional  
262 feature of tropospheric ozone seasonality, not represented from the climatological data in which long-term  
263 global measurements are composited as a function of month and latitude.

264 Both MERRA-2 and CAMS considerably overestimate ozone abundances in both troposphere and  
265 stratosphere in spite of that MLS measurements are commonly employed for assimilating stratospheric  
266 ozone profiles. In MERRA-2, the bimodal peaks (April and October) of the lower tropospheric ozone is  
267 inconsistent with others (early summer, September). We also compare how each ozone product represents  
268 the tropopause against thermally defined tropopause heights using the World Meteorological Organization  
269 (WMO) definition (WMO, 1957). There is no universal method to define the ozonepause height, but  
270 threshold values of 100 to 150 ppb in ozone mixing ratios were used to discriminate stratospheric to  
271 tropospheric air masses (e.g., Hsu et al., 2005; Prather et al., 2011). In this paper, the 150 ppb value is

272 selected due to similarities of thermal tropopauses with ozone surfaces of 150 hPa from ozonesonde  
 273 measurements. As shown, the ozone surfaces at 150 ppb of reanalysis products are positioned in the free  
 274 troposphere due to the overestimation errors. Both ozonesonde and Aura measurements show somewhat  
 275 consistency between their ozone and thermal tropopause pressures. In particular, OMI shows the strong  
 276 consistency with the fact that retrievals near the tropopause are largely constrained with the a priori state  
 277 taken from the tropopause-based ozone profile climatology (Bak et al., 2013).



278  
 279 **Figure 5.** Contour plots of monthly ozone profiles in 2020 from (a) ozonesonde, (b) MLS, (c) OMI, (d)

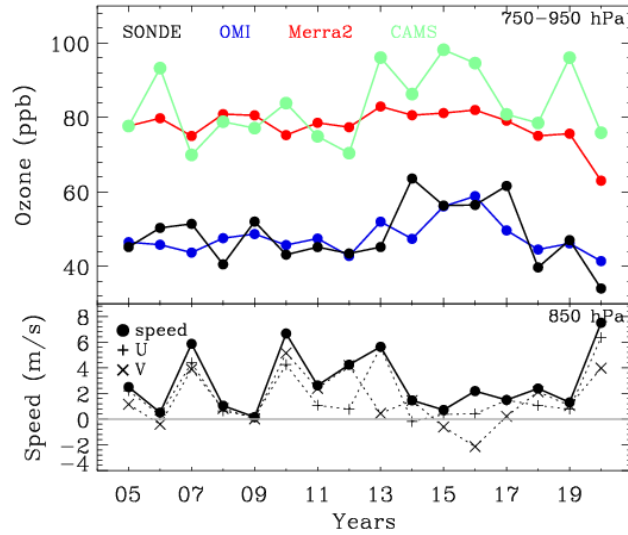
280 OMI a priori, (e) MERRA-2, and (f) CAMS. The meteorological variables are superimposed for wind barbs  
281 (red symbols), potential temperatures (black contours), thermal tropopause heights (white lines) using  
282 monthly MERRA-2 meteorological data. The ozone value of 150 ppb is plotted with green lines for  
283 indicating the chemical transition between troposphere and stratosphere.

### 284 **3.3. Interannual variability of lower tropospheric ozone in summer**

285 In this section, we focus on the ozone changes related to interannual meteorological variabilities, along  
286 with the evaluation of different ozone products. In Figure 6, the time-series of mean ozone mixing ratio in  
287 the lower troposphere (750-950 hPa) in August are compared. The summer monsoon typically ends in the  
288 late July and early August over Korean peninsula and hence the ozone abundance in August is sensitive to  
289 the intensity and duration of the monsoon season. OMI and ozonesonde show a similar long-term change,  
290 except for much more fluctuations in time-series of ozonesondes due to insufficient samplings (weekly  
291 observations) used in monthly averages. A noticeable correlation ( $r \sim -0.52$ ) exists between wind speeds  
292 and ozone mixing ratios (ozonesonde). Low wind speed could enhance the accumulation of ozone  
293 precursors and the rate of ozone formation. Accordingly, both ozonesonde and OMI measurements detect  
294 higher ozone abundances in August from 2014 to 2017 when the wind speeds are relatively lower. As  
295 shown in Figure 7 (a-c), where the monthly meteorological fields at 850 hPa in 2015 are presented from  
296 MERRA-2 product, the western North Pacific Subtropical High (WNPSH) was broken in August and hence  
297 the weather was likely to be calm and dry over the Korean peninsula. Compared to past few years, the lower  
298 amount of ozone is detected in 2020 from ozonesonde measurements. In August 2020, the lower  
299 tropospheric southwesterly winds blow from the western North Pacific to Korean Peninsula across the edge  
300 of WNPSH as well as the rain belt was activated over Korean Peninsula (Fig. 7. d-f). Therefore, the weather  
301 was windy and wet, suppressing ozone formation in August 2020.

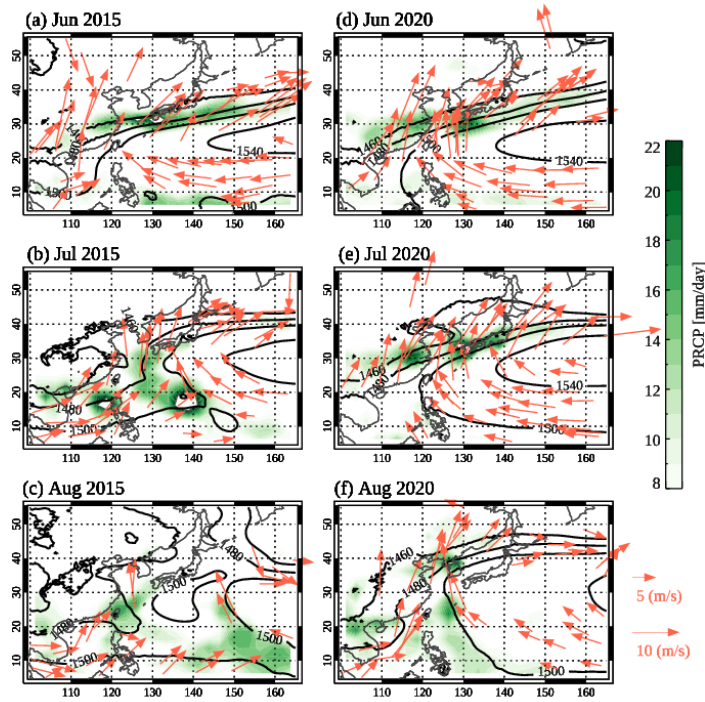
302 MERRA-2 ozone shows no annual variation, before 2020 unlike other ozone measurements and product.  
303 CAMS also shows the higher ozone concentrations correlated with wind speeds, but less consistent with  
304 ozonesonde measurements compared to OMI. How the El Niño-Southern Oscillation (ENSO) cycle  
305 interacts with the East Asian monsoon has been not established. According to the Oceanic Niño Index, the  
306 2015-2016 El Niño event, the warm phase of the ENSO, was one of the strongest events ever recorded,  
307 whereas the 2020-2021 La Niña event was also abnormally strong. There was a lot of unprecedented  
308 weather events in south Korea during these super El Niño and La Niña periods, such as  
309 unprecedented summer rainfalls in 2020 and unprecedented summer heatwaves in 2015-2016 (Yoon et al.,  
310 2018). Therefore, we could relate the higher ozone amount in August 2015-2017 and the lower ozone  
311 amount in August 2020 to a climatic forcing on the strength and position of WNPSH and hence the East

312 Asian summer climate.



313

314 **Figure 6.** Annual variations of (top) the lower tropospheric ozone (750-950 hPa) in August from various  
315 ozone products, along with (bottom) the wind speeds at 850 hPa.



316

317 **Figure 7.** The monthly meteorological fields at 850 hPa for (a-c) 2015 and (d-f) 2020, respectively. The wind vectors  
318 are drawn with the orange arrows. The geopotential heights are superimposed with black lines. The variations of  
319 precipitation are shown with green typed colors, respectively. Note that we use MERRA-2 meteorological variables

320 except for the precipitation data taken from GPCP Version 2.3 Combined Precipitation Data Set (Adler et al., 2003).

321

## 322 **4 Summary and Conclusions**

323 In this paper, atmospheric ozone variabilities over Korean peninsula and their linkages to the East  
324 Asian summer monsoon are vertically characterized using multiple ozone measurements made by surface  
325 observation, balloon-borne ozonesonde, OMI, and MLS. MERRA-2 and CAMS are also integrated in this  
326 analysis for the evaluation against ozonesonde. Surface in-situ measurements at six urban sites in Pohang  
327 are averaged, while satellite and reanalysis datasets are spatially interpolated onto the Pohang ozonesonde  
328 site. Surface measurements clearly show the impact of frequent weather changes (dry and wet) on ozone  
329 concentrations in spring. The seasonality of ozone becomes very complicated in late spring to early fall,  
330 depending on monsoon strengths and lengths. The peak concentration of ozone occurs in the pre-summer  
331 monsoon season (~ 70 ppb) and in the post-summer monsoon season (~50 ppb). During the summer  
332 monsoon, ozone concentrations decrease down to ~ 30 ppb, which is even lower than that in the winter  
333 when the air temperature and solar insolation is lowest. The vertical structures of ozone concentrations  
334 driven by the stratospheric dynamics and synoptic scale tropospheric weather disturbances are  
335 characterized from ozonesonde soundings. The stratospheric intrusions actively occur from March to May  
336 and modulate the upper tropospheric ozone, down to ~ 300 hPa. We identified ozone enhancements in the  
337 boundary layer, extending up to 400 hPa in June. In August the monsoon-induced ozone dilution occurs in  
338 the lower troposphere up to ~ 600 hPa. The ozone minimum also occurs just below the tropopause, which  
339 is deepest from summer to early fall with the troposphere being extending upward to ~ 100 hPa. Both  
340 satellite and reanalysis datasets show the capability of reproducing general features of ozone seasonality  
341 such as bimodal peaks in ground-level ozone and spring maximum in the UTLS ozone. However, MERRA-  
342 2 and CAMS products significantly overestimates ozone abundances in the UTLS and hence middle  
343 tropospheric ozone concentrations exceed 150 ppb which is used as a chemical proxy to distinguish between  
344 stratospheric air and tropospheric air. In general, OMI shows a good agreement with ozonesonde  
345 measurements with respect to both seasonal tendency and quantitative terms, but slightly underestimates  
346 ground-level ozone due to the limited vertical sensitivity. The lower tropospheric ozone in August shows  
347 the monsoon-induced interannual variabilities with higher concentrations during the super El Niño and  
348 lower concentration during the significant La Niña period, commonly from ozonesonde and OMI  
349 measurements. However, MERRA-2 rarely shows long-term changes of August ozone in the lower  
350 troposphere. On the other hand, CAMS is annually correlated with ozonesonde measurements, but with the

351 systematic positive biases of ~ 40 ppb. In conclusion, OMI could play a vital role in studying the impact of  
352 summer monsoon-derived atmospheric circulation and weather on ozone seasonality. The analysis results  
353 of this study could be a useful reference to the upcoming results from the ACCLIP campaign planned in  
354 the summer of 2022 to gather comprehensive, integrated datasets of two airborne observations (Flight  
355 Operations from S. Korea) and ground/balloon measurements, over the East Asia and Western Pacific.  
356 ACCLIP measurements will provide useful ideas for better understanding the spatiotemporal variation of  
357 ozone in the Korean peninsula in terms of continuous ozone increase near the surface (Yoo et al., 2015),  
358 high ozone in the free troposphere (Crawford et al., 2021), and the relationship between the stratospheric  
359 ozone intrusion and atmospheric circulation (Park et al., 2012).

360

361 **Author Contributions** J.B and C.K designed the research; E.S interpreted the reanalysis products  
362 and H.L and W.J contributed on analyzing surface measurements. X.L contributed on OMI ozone profile  
363 retrievals. C.K and J.H.K (JaeHwan Kim) provided oversight and guidance for connecting the weather  
364 condition and air pollutant concentrations. J.H.K (JaHo Koo) and J.W.K (Joowan Kim) contributed to the  
365 interpretation of the results. J.B lead the writing of the manuscript; all co-authors contributed to discussion  
366 and edited the paper.

367 **Competing interests.** The authors have no competing interests

## 368 **Acknowledgement**

369 We thank the KMA, NIER, NASA, and Copernicus for providing their measurements and analysis data.  
370 We hope that the 2022 ACCLIP campaign could successfully be processed in South Korea and the research  
371 outcome would be fascinating. We would like to acknowledge the Basic Science Research Program  
372 (2020R1A6A1A03044834 and 2021R1A2C1004984).

373 *Financial support.* This research has been supported by the Basic Science Research Program through the  
374 National Research Foundation of Korea (NRF) funded by the Ministry of Education (grant  
375 no. 2020R1A6A1A03044834 and 2021R1A2C1004984)

## 376 **Data Availability**

377 Ozonesonde: <https://data.kma.go.kr> (last access: 14 Oct 2022)  
378 AirKorea: <http://www.airkorea.or.kr> (last access: 14 Oct 2022)  
379 ASOS: <https://data.kma.go.kr> (last access: 14 Oct 2022)

380 OMI ozone profile retrievals: attainable upon request (juseonbak@pusan.ac.kr)  
381 MLS Version 4.2 ozone profile: <https://earthdata.nasa.gov> (last access: 16 Jun 2022).  
382 MERRA-2 reanalysis data: <https://gmao.gsfc.nasa.gov/reanalysis/MERRA-2/> (last access: 14 Oct 2022).  
383 CAMS global reanalysis (EAC4): <https://ads.atmosphere.copernicus.eu/> (last access: 14 Oct 2022).  
384 GPCP Version 2.3 Combined Precipitation Data Set: <https://psl.noaa.gov/> (last access: 14 Oct 2022)  
385

## 386 **References**

387  
388 Bak, J., Liu, X., Wei, J. C., Pan, L. L., Chance, K. and Kim, J. H.: Improvement of omi ozone profile  
389 retrievals in the upper troposphere and lower stratosphere by the use of a tropopause-based ozone  
390 profile climatology, *Atmos. Meas. Tech.*, 6(9), 2239–2254, doi:10.5194/amt-6-2239-2013, 2013.  
391 Bak, J., Baek, K.-H., Kim, J.-H., Liu, X., Kim, J. and Chance, K.: Cross-evaluation of GEMS  
392 tropospheric ozone retrieval performance using OMIData and the use of an ozonesonde dataset over  
393 East Asia for validation, *Atmos. Meas. Tech.*, 12(9), 5201–5215, doi:10.5194/amt-12-5201-2019,  
394 2019.  
395 Choi, J.-W., Kim, H.-D. and Wang, B.: Interdecadal variation of Changma (Korean summer monsoon  
396 rainy season) retreat date in Korea, *Int. J. Climatol.*, 40(3), 1348–1360,  
397 doi:<https://doi.org/10.1002/joc.6272>, 2020.  
398 Crawford, J. H., Ahn, J.-Y., Al-Saadi, J., Chang, L., Emmons, L. K., Kim, J., Lee, G., Park, J.-H., Park,  
399 R. J., Woo, J. H., Song, C.-K., Hong, J.-H., Hong, Y.-D., Lefer, B. L., Lee, M., Lee, T., Kim, S., Min,  
400 K.-E., Yum, S. S., Shin, H. J., Kim, Y.-W., Choi, J.-S., Park, J.-S., Szykman, J. J., Long, R. W.,  
401 Jordan, C. E., Simpson, I. J., Fried, A., Dibb, J. E., Cho, S. and Kim, Y. P.: The Korea–United States  
402 Air Quality (KORUS-AQ) field study, *Elem. Sci. Anthr.*, 9(1), doi:10.1525/elementa.2020.00163,  
403 2021.  
404 Dufour, G., Hauglustaine, D., Zhang, Y., Eremenko, M., Cohen, Y., Gaudel, A., Siour, G., Lachatre, M.,  
405 Bense, A., Bessagnet, B., Cuesta, J., Ziemke, J., Thouret, V. and Zheng, B.: Recent ozone trends in the  
406 Chinese free troposphere: role of the local emission reductions and meteorology, *Atmos. Chem. Phys.*,  
407 21(20), 16001–16025, doi:10.5194/acp-21-16001-2021, 2021.  
408 Gao, L., Wang, T., Ren, X., Ma, D., Zhuang, B., Li, S., Xie, M., Li, M. and Yang, X.-Q.: Subseasonal  
409 characteristics and meteorological causes of surface O<sub>3</sub> in different East Asian summer monsoon  
410 periods over the North China Plain during 2014–2019, *Atmos. Environ.*, 264, 118704,  
411 doi:<https://doi.org/10.1016/j.atmosenv.2021.118704>, 2021.  
412 Gelaro, R., McCarty, W., Suárez, M. J., Todling, R., Molod, A., Takacs, L., Randles, C., Darmenov, A.,  
413 Bosilovich, M. G., Reichle, R., Wargan, K., Coy, L., Cullather, R., Draper, C., Akella, S., Buchard, V.,  
414 Conaty, A., da Silva, A., Gu, W., Kim, G.-K., Koster, R., Lucchesi, R., Merkova, D., Nielsen, J. E.,  
415 Partyka, G., Pawson, S., Putman, W., Rienecker, M., Schubert, S. D., Sienkiewicz, M. and Zhao, B.:  
416 The Modern-Era Retrospective Analysis for Research and Applications, Version 2 (MERRA-2), *J.*  
417 *Clim.*, Volume 30(Iss 13), 5419–5454, doi:10.1175/JCLI-D-16-0758.1, 2017.  
418 Gettelman, A., Hoor, P., Pan, L. L., Randel, W. J., Hegglin, M. I. and Birner, T.: THE  
419 EXTRATROPICAL UPPER TROPOSPHERE AND LOWER STRATOSPHERE, *Rev. Geophys.*,  
420 49(3), doi:<https://doi.org/10.1029/2011RG000355>, 2011.  
421 Ha, K.-J., Heo, K.-Y., Lee, S.-S., Yun, K.-S. and Jhun, J.-G.: Variability in the East Asian Monsoon: a  
422 review, *Meteorol. Appl.*, 19(2), 200–215, doi:<https://doi.org/10.1002/met.1320>, 2012.  
423 He, Y. J., Uno, I., Wang, Z. F., Pochanart, P., Li, J. and Akimoto, H.: Significant impact of the East Asia  
424 monsoon on ozone seasonal behavior in the boundary layer of Eastern China and the west Pacific  
425 region, *Atmos. Chem. Phys.*, 8(24), 7543–7555, doi:10.5194/acp-8-7543-2008, 2008.  
426 Hsu, J., Prather, M. J. and Wild, O.: Diagnosing the stratosphere-to-troposphere flux of ozone in a



427 chemistry transport model, *J. Geophys. Res. Atmos.*, 110(D19),  
 428 doi:<https://doi.org/10.1029/2005JD006045>, 2005.

429 Inness, A., Ades, M., Agustí-Panareda, A., Barré, J., Benedictow, A., Blechschmidt, A.-M.,  
 430 Dominguez, J. J., Engelen, R., Eskes, H., Flemming, J., Huijnen, V., Jones, L., Kipling, Z., Massart,  
 431 S., Parrington, M., Peuch, V.-H., Razinger, M., Remy, S., Schulz, M. and Suttie, M.: The CAMS  
 432 reanalysis of atmospheric composition, *Atmos. Chem. Phys.*, 19(6), 3515–3556, doi:10.5194/acp-19-  
 433 3515-2019, 2019.

434 Jacob, D. J. and Winner, D. A.: Effect of climate change on air quality, *Atmos. Environ.*, 43(1), 51–63,  
 435 doi:<https://doi.org/10.1016/j.atmosenv.2008.09.051>, 2009.

436 Kley, D. and McFarland, M.: Chemiluminescence detector for NO and NO<sub>2</sub>, 1980.

437 Langford, A. O., Senff, C. J., Alvarez, R. J., Brioude, J., Cooper, O. R., Holloway, J. S., Lin, M. Y.,  
 438 Marchbanks, R. D., Pierce, R. B., Sandberg, S. P., Weickmann, A. M. and Williams, E. J.: An  
 439 overview of the 2013 Las Vegas Ozone Study (LVOS): Impact of stratospheric intrusions and long-  
 440 range transport on surface air quality, *Atmos. Environ.*, 109, 305–322,  
 441 doi:<https://doi.org/10.1016/j.atmosenv.2014.08.040>, 2015.

442 Li, S., Wang, T., Huang, X., Pu, X., Li, M., Chen, P., Yang, X.-Q. and Wang, M.: Impact of East Asian  
 443 Summer Monsoon on Surface Ozone Pattern in China, *J. Geophys. Res. Atmos.*, 123(2), 1401–1411,  
 444 doi:<https://doi.org/10.1002/2017JD027190>, 2018.

445 Liu, X., Bhartia, P. K., Chance, K., Spurr, R. J. D. and Kurosu, T. P.: Ozone profile retrievals from the  
 446 Ozone Monitoring Instrument, *Atmos. Chem. Phys.*, 10(5), 2521–2537, doi:10.5194/acp-10-2521-  
 447 2010, 2010.

448 Lu, X., Zhang, L. and Shen, L.: Meteorology and Climate Influences on Tropospheric Ozone: a Review  
 449 of Natural Sources, Chemistry, and Transport Patterns, *Curr. Pollut. Reports*, 5(4), 238–260,  
 450 doi:10.1007/s40726-019-00118-3, 2019.

451 Park, S. S., Kim, J., Cho, H. K., Lee, H., Lee, Y. and Miyagawa, K.: Sudden increase in the total ozone  
 452 density due to secondary ozone peaks and its effect on total ozone trends over Korea, *Atmos. Environ.*,  
 453 47, 226–235, doi:<https://doi.org/10.1016/j.atmosenv.2011.11.011>, 2012.

454 Prather, M. J., Zhu, X., Tang, Q., Hsu, J. and Neu, J. L.: An atmospheric chemist in search of the  
 455 tropopause, *J. Geophys. Res. Atmos.*, 116(D4), doi:<https://doi.org/10.1029/2010JD014939>, 2011.

456 Rao, T. N., Kirkwood, S., Arvelius, J., von der Gathen, P. and Kivi, R.: Climatology of UTLS ozone and  
 457 the ratio of ozone and potential vorticity over northern Europe, *J. Geophys. Res. Atmos.*, 108(D22),  
 458 doi:<https://doi.org/10.1029/2003JD003860>, 2003.

459 Rodgers, C. D.: *Inverse Methods for Atmospheric Sounding*, WORLD SCIENTIFIC., 2000.

460 Shen, L., Jacob, D. J., Liu, X., Huang, G., Li, K., Liao, H. and Wang, T.: An evaluation of the ability of  
 461 the Ozone Monitoring Instrument (OMI) to observe boundary layer ozone pollution across China:  
 462 application to 2005–2017 ozone trends, *Atmos. Chem. Phys.*, 19(9), 6551–6560, doi:10.5194/acp-19-  
 463 6551-2019, 2019.

464 Shen, L., Liu, J., Zhao, T., Xu, X., Han, H., Wang, H. and Shu, Z.: Atmospheric transport drives regional  
 465 interactions of ozone pollution in China, *Sci. Total Environ.*, 830, 154634,  
 466 doi:<https://doi.org/10.1016/j.scitotenv.2022.154634>, 2022.

467 Smit, H., Straeter, W., Johnson, B. J. J., Oltmans, S. J., Davies, J., Tarasick, D. W., Hoegger, B., Stübi,  
 468 R., Schmidlin, F. J., Northam, T., Thompson, A. M., Witte, J. C., Boyd, I. and Posny, F.: Assessment  
 469 of the performance of ECC-ozonesondes under quasi-flight conditions in the environmental simulation  
 470 chamber: Insights from the Juelich Ozone Sonde Intercomparison Experiment (JOSIE), *J. Geophys.*  
 471 *Res.*, 112, 2007.

472 Walker, T. W., Martin, R. V., Van Donkelaar, A., Leaitch, W. R., MacDonald, A. M., Anlauf, K. G.,  
 473 Cohen, R. C., Bertram, T. H., Huey, L. G., Avery, M. A., Weinheimer, A. J., Flocke, F. M., Tarasick,  
 474 D. W., Thompson, A. M., Streets, D. G. and Liu, X.: Trans-pacific transport of reactive nitrogen and

475 ozone to Canada during spring, *Atmos. Chem. Phys.*, 10(17), 8353–8372, doi:10.5194/acp-10-8353-  
476 2010, 2010.

477 WMO (World Meteorological Organization): METEOROLOGICAL At all modern meteorological  
478 stations THE PRECISION INSTRUMENTS OF, *WMO Bull.*, VI(4), 1957.

479 Worden, J., Jones, D. B. A., Liu, J., Parrington, M., Bowman, K., Stajner, I., Beer, R., Jiang, J., Thouret,  
480 V., Kulawik, S., Li, J.-L. F., Verma, S. and Worden, H.: Observed vertical distribution of tropospheric  
481 ozone during the Asian summertime monsoon, *J. Geophys. Res. Atmos.*, 114(D13),  
482 doi:<https://doi.org/10.1029/2008JD010560>, 2009.

483 Yang, Y., Liao, H. and Li, J.: Impacts of the East Asian summer monsoon on interannual variations of  
484 summertime surface-layer ozone concentrations over China, *Atmos. Chem. Phys.*, 14(13), 6867–6879,  
485 doi:10.5194/acp-14-6867-2014, 2014.

486 Yin, C. Q., Solmon, F., Deng, X. J., Zou, Y., Deng, T., Wang, N., Li, F., Mai, B. R. and Liu, L.:  
487 Geographical distribution of ozone seasonality over China, *Sci. Total Environ.*, 689, 625–633,  
488 doi:<https://doi.org/10.1016/j.scitotenv.2019.06.460>, 2019.

489 Yoo, J.-M., Jeong, M.-J., Kim, D., Stockwell, W. R., Yang, J.-H., Shin, H.-W., Lee, M.-I., Song, C.-K.  
490 and Lee, S.-D.: Spatiotemporal variations of air pollutants (O<sub>3</sub>, NO<sub>2</sub>, SO<sub>2</sub>, CO,  
491 PM<sub>10</sub>, and VOCs) with land-use types, *Atmos. Chem. Phys.*, 15(18), 10857–10885,  
492 doi:10.5194/acp-15-10857-2015, 2015.

493 Yoon, D., Cha, D.-H., Lee, G., Park, C., Lee, M.-I. and Min, K.-H.: Impacts of Synoptic and Local  
494 Factors on Heat Wave Events Over Southeastern Region of Korea in 2015, *J. Geophys. Res. Atmos.*,  
495 123(21), 12,12-81,96, doi:<https://doi.org/10.1029/2018JD029247>, 2018.

496 Zhang, Y. and Wang, Y.: Climate-driven ground-level ozone extreme in the fall over the Southeast  
497 United States, *Proc. Natl. Acad. Sci.*, 113(36), 10025–10030, doi:10.1073/pnas.1602563113, 2016.

498 Zhao, C., Wang, Y., Yang, Q., Fu, R., Cunnold, D. and Choi, Y.: Impact of East Asian summer monsoon  
499 on the air quality over China: View from space, *J. Geophys. Res. Atmos.*, 115(D9),  
500 doi:<https://doi.org/10.1029/2009JD012745>, 2010.

501 Zhou, Y., Yang, Y., Wang, H., Wang, J., Li, M., Li, H., Wang, P., Zhu, J., Li, K. and Liao, H.: Summer  
502 ozone pollution in China affected by the intensity of Asian monsoon systems, *Sci. Total Environ.*, 849,  
503 157785, doi:<https://doi.org/10.1016/j.scitotenv.2022.157785>, 2022.

504

505 Schwartz, M., Froidevaux, L., Livesey, N. and Read, W. (2015), MLS/Aura Level 2 Ozone (O<sub>3</sub>) Mixing  
506 Ratio V004, Greenbelt, MD, USA, Goddard Earth Sciences Data and Information Services Center  
507 (GES DISC), Accessed: [last access: 14 Oct 2022], 10.5067/Aura/MLS/DATA2017

508 Adler, R.F., G.J. Huffman, A. Chang, R. Ferraro, P. Xie, J. Janowiak, B. Rudolf, U. Schneider, S. Curtis,  
509 D. Bolvin, A. Gruber, J. Susskind, and P. Arkin: The Version 2 Global Precipitation Climatology  
510 Project (GPCP) Monthly Precipitation Analysis (1979-Present). *J. Hydrometeor.*, 4,1147-1167,  
511 2003

512